Search for spontaneous conversion of muonium to antimuonium

B. Ni,[a,*] K.-P. Arnold,[a,†] F. Chmely,[a] M. D. Cooper,[b] M. Eckhause,[c] P. P. Guss,[c,‡]
C. M. Hoffman,[b] G. E. Hogan,[b] V. W. Hughes,[a] J. R. Kane,[c] S. H. Kettell,[a,§] Y. Kuang,[a,‖] J. Markey,[a]
B. E. Matthias,[a,¶] R. E. Mischke,[b] H. Orth,[a,**] L. E. Piilonen,[b,††] G. zu Putlitz,[d] J. Reidy,[e] H. R. Schaefer,[a]
R. A. Williams,[b] and K. A. Woodle[a,‡‡]

[a]*Yale University, New Haven, Connecticut 06511*
[b]*Los Alamos National Laboratory, Los Alamos, New Mexico 87545*
[c]*College of William and Mary, Williamsburg, Virginia 23185*
[d]*Universität Heidelberg, D-6900 Heidelberg, Germany*
[e]*University of Mississippi, University, Mississippi 38677*

(Received 9 November 1992)

An experimental search for the spontaneous conversion of muonium to antimuonium is described. A 10 MeV/c μ^+ beam of average intensity 3×10^5 s^{-1} was used to produce muonium atoms in vacuum by charge capture in a thin foil. The novel method applied here for detection of an antimuonium atom was a triple coincidence of two muonic x-ray photons from the atomic capture of its μ^- by a high-Z target and a secondary electron ejected from the target upon the impact of the antimuonium atom. No antimuonium events were observed and the resulting 90% confidence level upper limit on the coupling constant leading to the conversion, $G_{M\bar{M}}$, is $6.9G_F$, where G_F is the Fermi coupling constant.

PACS number(s): 36.10.Dr, 13.10.+q, 13.35.+s, 14.60.−z

I. INTRODUCTION

The possibility of muonium (M or μ^+e^-) to antimuonium ($\bar{M}$ or μ^-e^+) conversion was first suggested by Pontecorvo [1] in 1957 in analogy with the ($K^0,\bar{K}^0$) system in which a particle-antiparticle mixing occurs by the weak interaction. Further early discussions of this process [2] were related to the applicability of two different versions of a lepton number conservation law. While forbidden by the additive lepton number conservation law [3–5] (Table I), the $M\rightarrow\bar{M}$ conversion is allowed by the multiplicative lepton number conservation law [2] (Table II). The minimum standard model of the unified electroweak interaction [6–8] incorporates the additive law as an empirical fact without deeper motivation. Left-right-symmetric extensions [9–11], on the other hand, suggest the existence of massive Majorana neutrinos and of additional Higgs bosons [12] that might mediate the $M\rightarrow\bar{M}$ conversion. From the diagrams shown in Fig. 1 and the experimental data obtained from nuclear neutrinoless double β decay [13], the value of $G_{M\bar{M}}$, the coupling constant leading to the $M\rightarrow\bar{M}$ conversion, is estimated to be, at most, $10^{-5}G_F$ for the Majorana-neutrino-mediated process and to be as large as $10G_F$ for the doubly charged Higgs boson exchange process [14], where G_F is the Fermi coupling constant. However, the uncertainties in the model parameters should be emphasized, rendering these theoretical estimates quite speculative. In general, a sensitive experimental search for the $M\rightarrow\bar{M}$ conversion is important as it offers additional constraints on extensions to the standard model

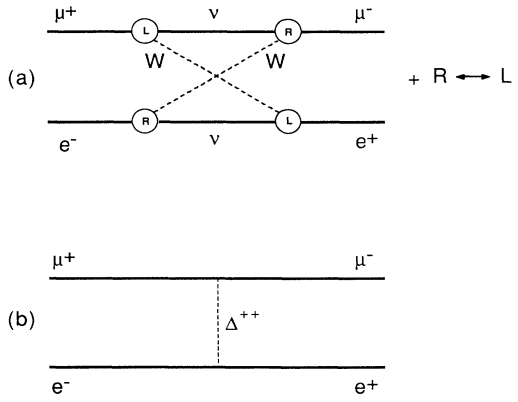

FIG. 1. Diagrams for (a) Majorana-neutrino and (b) Higgs-boson-induced $M\rightarrow\bar{M}$ conversion.

*Present address: IUCF, 2401 Milo B. Sampson Lane, Bloomington, IN 47408.
†Present address: Firma ANT, D-7150 Backnang, Germany.
‡Present address: EG&G Energy Measurements, Box 380, Suitland, MD 20746.
§Present address: Temple University, Philadelphia, PA 19122.
‖Present address: College of William and Mary, Williamsburg, Virginia 23185.
¶Present address: Universität Heidelberg, D-6900 Heidelberg, Germany.
**Present address: Gesellschaft für Schwerionenforschung, D-6100 Darmstadt, Germany.
††Present address: Department of Physics, Virginia Polytechnic Institute and State University, Blacksburg, VA 24061.
‡‡Present address: Brookhaven National Laboratory, Upton, NY 11973.

TABLE I. The additive lepton number conservation law.

	Additive lepton number assignment								
	e^-	ν_e	e^+	$\bar{\nu}_e$	μ^-	ν_μ	μ^+	$\bar{\nu}_\mu$	All others
L_e	+1	+1	−1	−1	0	0	0	0	0
L_μ	0	0	0	0	+1	+1	−1	−1	0

Additive lepton number conservation law

$$\sum L_e = \text{const}$$
$$\sum L_\mu = \text{const}$$

Allowed:
$\mu^+ \to e^+ \nu_e \bar{\nu}_\mu$

Forbidden:
$\mu^+ \to e^+ \gamma$
$\mu^+ \to e^+ e^- e^+$
$\mu^- Z \to e^- Z$
$\mu^- Z \to e^+ (Z-2)$
$\mu^+ e^- \to \mu^- e^+$
$e^- e^- \to \mu^- \mu^-$
$\mu^+ \to e^+ \bar{\nu}_e \nu_\mu$

next to, for example, the searches for other rare muon decays ($\mu^+ \to e^+ \gamma$, $\mu^+ \to e^+ e^- e^+$, $\mu^- Z \to e^- Z$, $\mu^+ \to e^+ \bar{\nu}_e \nu_\mu$).

This is the complete report on an experiment to search for the spontaneous conversion of muonium to antimuonium that used a muonium beam in vacuum generated by the beam-foil method. Results have already been published [15]; a slightly improved result based on refined analysis is given here. After the first demonstration of the beam-foil technique of muonium production [16] it was immediately realized that a much higher sensitivity for the $M \to \bar{M}$ conversion process could be obtained with this approach than was achieved in previous experiments.

The first experiment searching for spontaneous $M \to \bar{M}$ conversion [17], conducted in 1968, used a stopped μ^+ beam from the Columbia Nevis synchrocyclotron to produce M atoms in a 1-atm Ar gas target. The signature for an $\bar{M}$ event was a μ^-Ar $K\alpha$ x ray (643 keV) unaccompanied by a decay positron. A 95% confidence level upper limit result of $G_{M\bar{M}} < 5800 G_F$ was established. The poor sensitivity of the result was partly due to the collisions of M atoms with Ar atoms, which break the $M, \bar{M}$ energy level degeneracy [18] and thus reduce the conversion probability by a factor of about 10^5.

Colliding electron beams at the Princeton-Stanford electron storage rings were used in 1969 to search [19] for the cross-channel reaction $e^- e^- \to \mu^- \mu^-$. This process and $M \to \bar{M}$ conversion should have the same coupling strength. No such events were found and a result of $G_{M\bar{M}} < 610 G_F$ (95% C.L.) was deduced.

Another experiment [20] was undertaken at TRIUMF in which a μ^+ beam was used to produce M atoms in a layered SiO_2 powder target supported by CaO coated collodion films. An $M \to \bar{M}$ conversion in vacuum drift regions between the target layers was searched for by detecting a 784-keV $K\alpha$ x ray from μ^-Ca. An upper limit on the coupling constant of $G_{M\bar{M}} < 42 G_F$ (95% C.L.) was first obtained in this experiment and revised [21] to $G_{M\bar{M}} < 20 G_F$ (95% C.L.) in 1986 after a reassessment of the muonium formation fraction in the SiO_2 powder.

At this time, a more sensitive probe for $M \to \bar{M}$ and an improvement on this upper limit on $G_{M\bar{M}}$ was made possible by several innovations implemented in the experiment discussed in this paper. Muonium atoms were produced in vacuum by the beam-foil method using a high-

TABLE II. The multiplicative lepton number conservation law.

	Multiplicative lepton number assignment.								
	e^-	ν_e	e^+	$\bar{\nu}_e$	μ^-	ν_μ	μ^+	$\bar{\nu}_\mu$	All others
L	+1	+1	−1	−1	+1	+1	−1	−1	0
P_μ	+1	+1	+1	+1	−1	−1	−1	−1	+1

Multiplicative lepton number conservation law

$$\sum L = \text{const}$$
$$\prod P_\mu = \text{const}$$

Allowed:
$\mu^+ \to e^+ \nu_e \bar{\nu}_\mu$
$\mu^+ e^- \to \mu^- e^+$
$e^- e^- \to \mu^- \mu^-$
$\mu^+ \to e^+ \bar{\nu}_e \nu_\mu$

Forbidden:
$\mu^+ \to e^+ \gamma$
$\mu^+ \to e^+ e^- e^+$
$\mu^- Z \to e^- Z$
$\mu^- Z \to e^+ (Z-2)$

intensity, low-momentum μ^+ beam. The availability of a large solid-angle detector for energetic photons enabled the efficient observation of coincident muonic x rays from a high-Z target. A further signature component was offered by the observation of the secondary electrons ejected from the target by the impact of M or $\overline{M}$ atoms. The threefold coincidence of two muonic x rays and a secondary electron pulse is then a stringent signature for the presence of an $\overline{M}$ atom which strongly suppresses accidental coincidences due to background processes.

Further significant improvements on the limit for $G_{M\overline{M}}$ were made possible by the recent development of a technique to produce thermal energy M atoms in vacuum with a high formation fraction [21–23]. Because thermal M atoms (a temperature of 300 K corresponds to a velocity of 0.7 cm/μs) typically travel only a few cm before they decay, searches for $M\rightarrow\overline{M}$ were realized allowing longer times for a possible conversion and affording more efficient detection of such an event [24,25]. The present best limit is due to an experiment at LAMPF performed subsequently to the one presently reported. Exploiting the advantages of thermal M in vacuum, $G_{M\overline{M}}<0.16G_F$ (90% C.L.) was established [25].

In this paper we give the full description of the earlier search for $M\rightarrow\overline{M}$ conversion using beam-foil muonium. After a brief summary in Sec. II of the quantum mechanics of $M\rightarrow\overline{M}$ conversion, Sec. III describes the apparatus with emphasis on the beam properties and the target design as well as on the detectors. The measurements and data analysis are described in Sec. IV. Section V gives the result for the upper limit on the $M\rightarrow\overline{M}$ coupling constant and a discussion of the limitations of the experimental method.

II. THE TIME-DEPENDENT $M,\overline{M}$ SYSTEM

Since the $\overline{M}$ signature of this experiment is sensitive to the $\overline{M}$ admixture of the coupled $M\leftrightarrow\overline{M}$ system at the time of impact on the target foil, we calculate the instantaneous probability of finding the system in the $\overline{M}$ state, given an initial state ($t=0$) of pure M in the $1S$ ground state. In the absence of external electromagnetic fields, M and $\overline{M}$ have the same ground-state energy levels as determined from a spin-dependent Hamiltonian $H_{\rm hf}=a\mathbf{S}_e\cdot\mathbf{S}_\mu$ which represents the interaction between the magnetic moments of $\mu^+(\mu^-)$ and $e^-(e^+)$ for $M(\overline{M})$. Here, $a=1.85\times10^{-5}$ eV is the zero-field ground-state hyperfine structure splitting in M and $\overline{M}$. Represented by $\mathbf{S}_\mu$ and $\mathbf{S}_e$ are the spin operators in units of $\hbar$ for μ^+ and e^-, respectively, when operating on M, and for μ^- and e^+, respectively, when operating on $\overline{M}$. The Coulomb term of the Hamiltonian is irrelevant to the further discussion of the $M\rightarrow\overline{M}$ conversion and hence is not carried further.

To represent the $M\rightarrow\overline{M}$ conversion, assuming a nonzero $G_{M\overline{M}}$, we make the conventional choice of a four-fermion Hamiltonian density of $V-A$ form to represent the $M\rightarrow\overline{M}$ conversion as a contact interaction:

$$\mathcal{H}_{M\overline{M}}=\frac{G_{M\overline{M}}}{\sqrt{2}}\bar{\psi}_\mu\gamma_\lambda(1+\gamma^5)\psi_e\bar{\psi}_\mu\gamma^\lambda(1+\gamma^5)\psi_e+\text{H.c.} \quad (1)$$

The corresponding Hamiltonian $H_{M\overline{M}}$ has diagonal matrix elements [26] coupling M with $\overline{M}$:

$$\langle\overline{M}(F,m_F)|H_{M\overline{M}}|M(F,m_F)\rangle \equiv\frac{\delta}{2}=(1.07\times10^{-12}\text{ eV})\frac{G_{M\overline{M}}}{G_F}\ . \quad (2)$$

In the presence of a magnetic field B, a Zeeman interaction term

$$H_Z=\mu_B g_e\mathbf{S}_e\cdot\mathbf{B}+\mu_B\frac{m_e}{m_\mu}g_\mu\mathbf{S}_\mu\cdot\mathbf{B} \quad (3)$$

must be added to $H_{\rm hf}$. For M, we know that $g_\mu=g_{\mu^+}\cong-2$ and $g_e=g_{e^-}\cong2$. For $\overline{M}$, the signs of the g factors are reversed, so $g_\mu=g_{\mu^-}\cong2$ and $g_e=g_{e^+}\cong-2$. Here, $\mu_B=5.79\times10^{-9}$ eV/G is the Bohr magneton, and m_e and m_μ are the electron and muon masses, respectively. Since $\overline{M}$ consists of the antiparticles of the constituents of M, the magnetic moment of the $\overline{M}$ atom is reversed in sign from that of M. The interaction H_Z removes the degeneracy of muonium and antimuonium energy levels and thus suppresses the $M\rightarrow\overline{M}$ conversion probability. In the following, $\mathbf{F}=\mathbf{S}_e+\mathbf{S}_\mu$, the eigenvalue F denotes the total angular momentum quantum number, and m_F is the angular momentum quantization along the direction of the external magnetic field.

At low magnetic fields where the fully coupled quantum numbers F and m_F are appropriate to specify the ground-state hyperfine levels, the energy levels with $m_F=\pm1$ in $\overline{M}$ exhibit the same magnetic field dependence as the $m_F=\mp1$ levels of M. Since the conversion coupling must conserve angular momentum, it is clear that conversions between the $m_F=\pm1$ levels are suppressed in the presence of an external magnetic field. To estimate the magnitude of the field that would lead to an appreciable effect, we compare the natural width of the levels with the energy difference of the $m_F=+1$ (or -1) levels in M and $\overline{M}$ (see closeup in Fig. 2). The condition

$$2\mu_B B=\frac{\hbar}{\tau} \quad (4)$$

gives $B=26$ mG, where $\tau\approx2.2$ μs is the mean lifetime of the muon. Thus, to enable conversions between M and $\overline{M}$ levels with $m_F=\pm1$, the $M(\overline{M})$ atoms must be carefully shielded from ambient magnetic fields.

Because the $m_F=0$ levels of M and $\overline{M}$ depend only weakly on the external field B, conversions between $m_F=0$ levels in M and $\overline{M}$ are not disturbed until B is large enough to begin to decouple the spins of the component particles of the atom. Though M and $\overline{M}$ with $m_F=0$ remain degenerate in energy with increasing fields, their spin states become orthogonal, thus inhibiting the $M\rightarrow\overline{M}$ conversion on grounds of angular momentum conservation (see Fig. 2). This occurs at fields on the order of [27]

$$B\approx\frac{a}{2\mu_B}=1.6\text{ kG}\ . \quad (5)$$

Conversions between the M and $\overline{M}$ levels with $m_F=0$ are, therefore, unaffected by the residual field in a carefully shielded apparatus.

To calculate rigorously the time-dependent behavior of the coupled $M \leftrightarrow \overline{M}$ system, one diagonalizes the full Hamiltonian of the system $H_{\rm hf}+H_Z+H_{M\overline{M}}$ in either the basis of fully uncoupled spins or in the basis of fully coupled spins. One obtains eight new eigenstates composed of M and $\overline{M}$ amplitudes whose relative strength is parametrically dependent on both the magnitude of the external field B and the $M \rightarrow \overline{M}$ coupling matrix element $\delta/2$. The initial state of pure M in our experiment may then be decomposed into a superposition of eigenstates of the combined M-$\overline{M}$ system. In this mathematical frame, the time evolution of a probability amplitude of $\overline{M}$ in a vacuum drift region can be calculated easily [18].

Further specifying the theoretical description to our experiment by including the fact that initially (at $t=0$) 50% of the M was in the $m_F=0$ states and 50% was in the $m_F=\pm 1$ states, we obtain [28], for the instantaneous probability of finding $\overline{M}$ at the time t,

$$P(\overline{M};t)=\frac{\delta^2}{8\mu_B^2 B^2}\sin^2\left[\frac{\mu_B B t}{\hbar}\right] + \frac{1}{2}\sin^2\left[\frac{\delta t}{2\hbar\sqrt{1+x^2}}\right]. \quad (6)$$

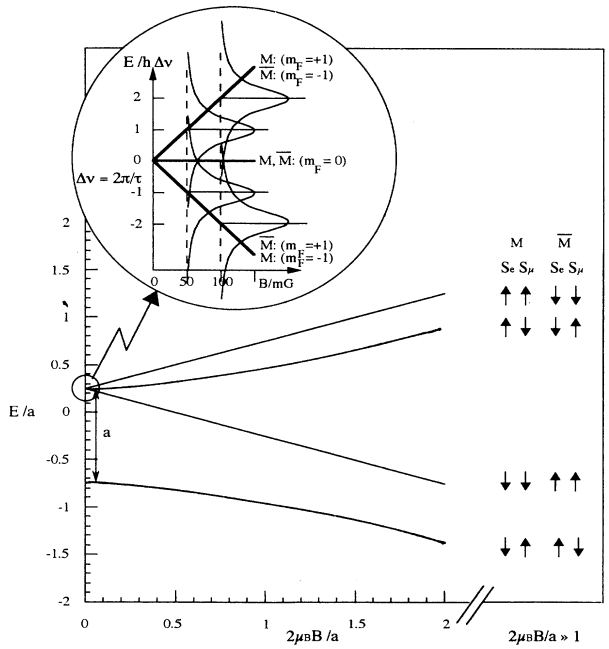

FIG. 2. Ground-state hyperfine energy levels in M and $\overline{M}$ vs external magnetic field. The eigenstates at high magnetic fields are given separately for M and $\overline{M}$ for each energy level and demonstrate the orthogonality of their atomic wave functions in this limit. The Zeeman triplet at low magnetic fields and the level broadening due to the muon lifetime is depicted in the inset. The suppression of $M \rightarrow \overline{M}$ conversion in this case is caused by the incomplete overlap of the participating levels.

Here, $x=6.31\times 10^{-4}B(\mathrm{G})$ is a parameter proportional to the external magnetic field. The coupling strength δ is assumed to be small compared to the spin-magnetic hyperfine coupling ($\delta/a \ll 1$). The first term in $P(\overline{M};t)$ comes from $(F=1,m_F=\pm 1)$ substates and reflects the sensitivity to the field B. The second term describes the conversion of $(F=1,m_F=0)$ and $(F=0,m_F=0)$ states, which is insensitive to the field as long as $x \ll 1$. In very weak external fields ($B \rightarrow 0$) we obtain

$$P(\overline{M};t)\approx\left[\frac{\delta t}{2\hbar}\right]^2 =\{2.6\times 10^{-6}[t(\mu\mathrm{s})]^2\}\left[\frac{G_{M\overline{M}}}{G_F}\right]^2. \quad (7)$$

Assuming $t=\tau$, $P(\overline{M};\tau)=1.3\times 10^{-5}(G_{M\overline{M}}/G_F)^2$.

The conversion probability is thus proportional to the square of the coupling constant, as expected, but the small leading factor makes a sensitive experiment difficult. This factor results partly from the small probability of overlap of the μ^+ and the e^- in muonium, a condition necessary for the conversion process to proceed as a contact interaction.

III. APPARATUS AND DETECTORS

The experiment was performed in 1986 at the Stopped Muon Channel [29] (SMC) of the Los Alamos Clinton P. Anderson Meson Physics Facility (LAMPF). A schematic diagram of the apparatus is shown in Fig. 3. A μ^+ beam of 10-MeV/c momentum and with an average intensity of $3\times 10^5 \mu^+$ s^{-1} was incident on a 20-μm-thick plastic scintillator followed by a 0.75-μm Al foil, in which forward-directed M with typical kinetic energies on the order of 15 keV was formed [30]. After traversing a 50-cm-long region with a magnetic bending power of 45 kG cm to sweep out the remaining μ^+, the M beam traveled in vacuum for a distance of 280 cm before striking a 1-μm-thick Bi target that was evaporated onto a 50-μm aluminized Mylar backing. The 45-cm-diam vacuum pipe was wrapped with three layers of 100-μm Co-Netic foil, mutually separated by two layers of 200-μm

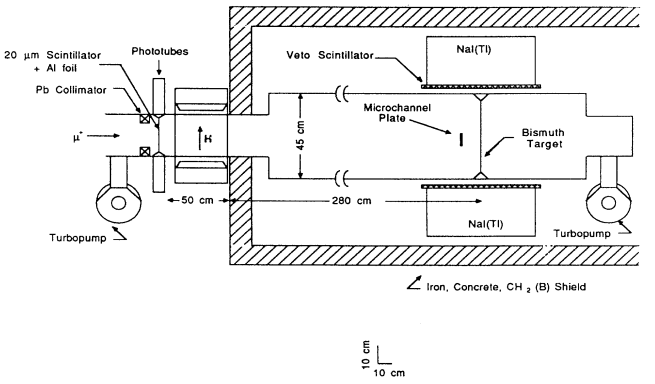

FIG. 3. Apparatus to search for $M \rightarrow \overline{M}$ conversion. For a detail of the target region see Fig. 7.

polyethylene sheets, to reduce the residual magnetic field in the M drift region. An average residual field of about 25 mG remained inside this pipe.

Muonium was formed at time $t=0$ and during its drift to the Bi target an admixture of $\overline{M}$ was allowed to develop. The probability that the system struck the Bi target while in the $\overline{M}$ state at time t is given by $P(\overline{M};t)$ of Eq. (6). An M atom stopping in Bi merely breaks up and the μ^+ decays, whereas an $\overline{M}$ atom immediately passes the μ^- over to the Coulomb field of a Bi nucleus, forming the muonic atom μ^-Bi. The $3d\rightarrow 2p$ ($L\alpha$) and $2p\rightarrow 1s$ ($K\alpha$) muonic x rays of the atomic capture cascade of μ^- on Bi were observed in coincidence and used to signal an $M\rightarrow\overline{M}$ conversion. The two photons were detected by a large array of NaI(Tl) crystals, the Crystal Box detector [31]. The characteristics of this large scintillator array, as relevant to this experiment, are explained in Sec. III D.

A microchannel plate (MCP), facing the Bi target and located 25 cm upstream of it, was used to monitor the secondary electrons emitted from the Bi target upon the impact of M or $\overline{M}$ atoms. This timing signal provided a direct measure of the number of M atoms that struck the Bi target. In the search for $\overline{M}$ atoms, it also provided an additional coincidence requirement, which greatly improved the signal-to-background ratio in the analysis.

The entire apparatus downstream of the sweeping magnet was placed within an enclosure of concrete blocks, iron plates, and borated polyethylene sheets [28] in order to shield the NaI crystals from accelerator correlated neutrons. Capture of a neutron on ^{127}I leads to a photon cascade including quanta with energies in the range of our $\overline{M}$ signature.

A. The muon beams

The LAMPF linear accelerator produces a pulsed proton beam of 800-MeV energy with average duty factor of 8% and an average current of 800 μA. The protons interact strongly with the nuclei of the A2 target, a 4-cm-thick spinning graphite disk, producing pions which subsequently decay into muons. A fraction of these muons are collected by the SMC, which views the A2 target at an angle of 65° to the proton beam with an acceptance of about 30 msr. Parity violation and angular momentum conservation in the decay $\pi\rightarrow\mu\nu$ causes these muons to be fully polarized.

For the main part of the experiment, the search for antimuonium, the muon channel was tuned to transport "subsurface μ^+" at 10-MeV/c momentum [32]. In connection with the time-of-flight measurements of muonium atoms (see Sec. III C) this muon momentum was further lowered to 8.2 MeV/c for technical reasons. For calibration of the response of the NaI crystals to the μ^-Bi atomic x rays, a different, polarity reversed tune was used to extract a μ^- beam at 19-MeV/c momentum.

The contamination of beam positrons (or electrons), from π^0 decay with subsequent $\gamma\rightarrow e^+e^-$ conversion and from muon decay in the channel, was substantially reduced by an $\mathbf{E}\times\mathbf{B}$ separator [32] that deflected all beam positrons (electrons) entering it, while fully transmitting the muon beam. A pair of quadrupole magnets downstream of the separator focused the muon beam onto the muonium production foil. Contamination in the channel from gaseous, radioactive spallation products [33] (^{12}N,^{6}He) originating from the hot graphite target was reduced by inserting a 1.5-μm Mylar gas barrier immediately downstream of the separator [32].

A 20-μm-thick (2.0 mg/cm^2), 7.6-cm-diam scintillator (NE102A, with a scintillation efficiency of 1 photon/140 eV deposited) coupled to four RCA 8850 photomultiplier tubes was used as a beam counter, capable of detecting single muons entering the apparatus. Its efficiency was more than 95% with a muon flux of $3\times10^5\mu^+$ s^{-1} at 10 MeV/c.

At a momentum of 19 MeV/c, muons have a range roughly five times larger than at 10 MeV/c and a correspondingly smaller specific energy loss in plastic scintillator. Therefore, to ensure that a 19-MeV/c μ^- deposits enough energy in the counter to give an ample scintillation pulse, the 20-μm-thick counter used at 10 MeV/c was replaced by one of 125 μm thickness for the higher momentum.

B. M formation in vacuum

This experiment employed the beam-foil technique [16] that has been used in several previous experiments to produce muonium in vacuum [34–36]. The 10-MeV/c muons partially stopped in the 0.75-μm Al foil which was attached to the downstream side of the beam counter. Muonium atoms emerged from the foil after the electron capture process.

The formation of M by the beam-foil method has been carefully studied in several experiments [30,16,37–39] and is a well-established technique. The most recent work [30] measured the energy and angular distributions of M and of μ^+ downstream of the production foil. This study verified experimentally that the beam-foil interaction of μ^+ is in agreement with the corresponding data for protons and deuterons [40–43], assuming the validity of velocity scaling. Since μ^+ must slow down to atomic velocities, corresponding to several keV of kinetic energy, to be able to capture efficiently an e^- at the downstream surface of the production foil, the M formation fraction is a sensitive function of the central momentum and the momentum spread of the incident μ^+ beam. Therefore, we optimized this incident momentum for maximal M production (see Fig. 4). Qualitatively, one may think of the M production optimum as that momentum for which the stopping distribution of μ^+ is centered on the downstream surface of the production foil, giving the highest possible μ^+ stopping density at this surface.

Typical M production fractions per incident μ^+ are on the order of 1%. These M atoms are mostly in the $1S$ state with fractions populating $2S$ and $2P$. The $2P$ M atoms rapidly decay to the $1S$ state (1.6 ns). Muonium in the $2S$ state is mixed with the $2P$ state by the strong motional electric field in the sweeping magnet and is, therefore, rapidly quenched to the $1S$ state (1.6 ns). Thus, all M atoms entering the conversion region are in the ground state. Independent of the muon polarization, the population of the substates with $m_F=0$ is equal to the

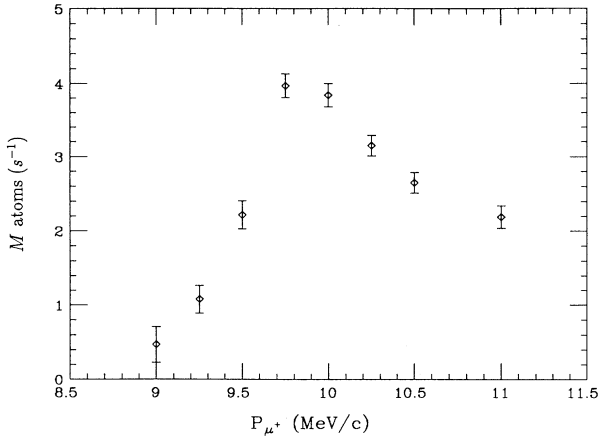

FIG. 4. Muonium rate at the Bi target as a function of the momentum of the muon beam.

sum of the populations of those with $m_F=+1$ and $m_F=-1$.

C. Time-of-flight of M from production foil to Bi target

A time-of-flight (TOF) measurement for M atoms traveling a distance of 174 cm was carried out in an auxiliary experiment in which the same M production foil was used. In this measurement, a low-pressure multiwire proportional chamber (MWPC) served as a beam counter with the M production foil attached to its downstream window. A MCP detector, placed 174 cm downstream of the MWPC, was used to stop the M atoms after μ^+ were swept out by a bending magnet. The TOF was measured with a LeCroy 4208 time-to-digital converter (TDC) which was started by the MCP pulse and stopped by the delayed MWPC pulse with a trigger which indicated the detection of both an M atom (by the MCP) and its decay positron (by a scintillator telescope). The result was then extrapolated to the case of a 340-cm flight path with a correction for M decay over the longer TOF. The result is plotted in Fig. 5 which shows an average TOF of about 1 μs. Subsequently, $\langle P(\bar{M})\rangle_t$ denotes the average of $P(\bar{M};t)$ weighted by this time-of-flight distribution and evaluated at the residual magnetic field of 25 mG. We obtain

$$\langle P(\bar{M})\rangle_t=(2.49\pm0.39)\times10^{-6}\left[\frac{G_{M\bar{M}}}{G_F}\right]^2. \quad (8)$$

The error in $\langle P(\bar{M})\rangle_t$ is due to the statistical uncertainties in the TOF distribution and the errors in the magnetic-field measurements.

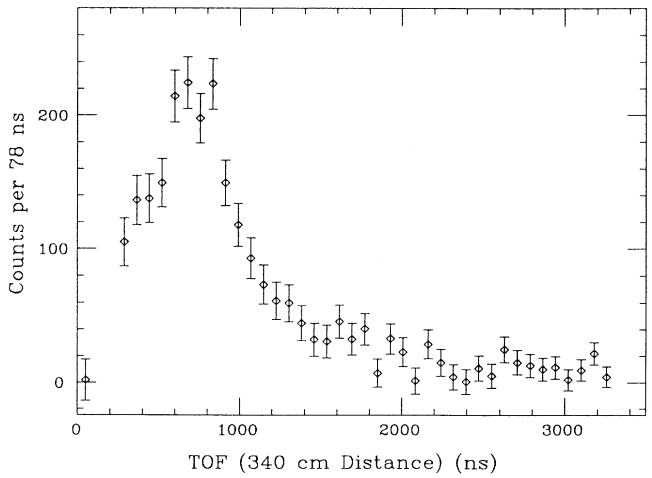

FIG. 5. Time-of-flight spectrum for M from the production foil to the Bi target.

D. Crystal Box detector

The Crystal Box detector (Fig. 6) had four identical quadrants, each consisting of 90 optically isolated "face" NaI(Tl) crystals (6.35 cm×6.35 cm×30 cm each), arranged into four "faces" of nine rows (parallel to the beam direction) and ten columns (transverse to the beam axis) each, and nine "corner" crystals (6.35 cm×6.35 cm×63.5 cm each). Based on the results of a Monte Carlo study [28] of detecting a muonic x-ray photon, the sum of the energies deposited in a 3×3 square cluster of face crystals, centered on the one with the highest pulse height, was defined as the photon energy. The energy leakage to the corner crystals could be neglected. The position and the timing of a photon were provided by the location and the timing of the central crystal of the cluster.

The energy scale of the NaI crystals was calibrated using a Pu-Be source that produced 4.4-MeV γ rays and a ^{24}Na source that yielded 2.7-MeV photons. To ensure the stability of the electronic gain in the NaI channels, each data acquisition run was prefaced by a "flasher run," in which light from a flash lamp of stable intensity

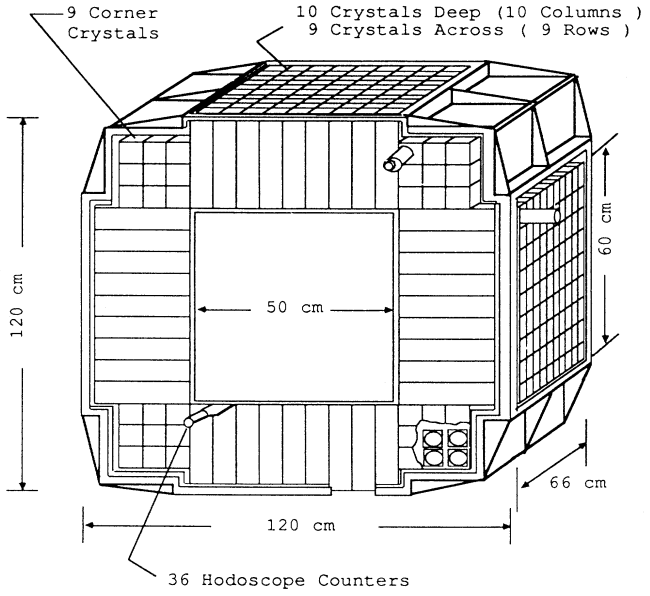

FIG. 6. The Crystal Box detector.

was carried to each photomultiplier on a NaI crystal by an optical fiber. Any electronic gain drift could then be detected and compensated in the off-line analysis. Stable and accurate timing on NaI signals was achieved by constant-fraction discrimination of the pulses from each crystal. An energy resolution of 16% [full width at half maximum (FWHM)] and a time resolution of ~ 4 ns (FWHM) for photons at ~ 6.0 MeV were measured using the muonic x-ray photons produced by a μ^- beam on the Bi target.

Thirty-six plastic scintillation hodoscope counters (44.5 cm $\times$ 5.7 cm $\times$ 1.27 cm each) covered the faces of NaI(Tl) crystals in order to distinguish between charged particles and photons and to provide the timing for charged particles. Each hodoscope counter was viewed by two photomultiplier tubes, one at each end. The pulses from these tubes went into constant-fraction discriminators followed by a meantimer, where the arrival times of the two signals were averaged so that the measured time was independent of the impact point on the hodoscope counter. The time resolution was typically better than 1 ns.

E. Trigger modes of the Crystal Box

To initiate a readout of the Crystal Box and the secondary electron detector, we made use of the two principal capabilities of the apparatus: the ability to distinguish between charged particles and photons and the coarse position sensitivity that is due to the modular architecture of the Crystal Box, as described in the previous section. The most important trigger modes for data taking were the so-called "2γ trigger" used for recording prospective muonic x-ray events (both during the $\overline{M}$ search and for observation of μ^-Bi x rays using a μ^- beam) and the "$1e$ trigger" that indicated the detection of an energetic e^+ from μ^+ or M decay.

A γ-ray detected in the Crystal Box was characterized by pulses in one or several neighboring NaI crystals in the absence of a correlated pulse in the hodoscope counter(s) covering these crystals. To simplify triggering on two photons with a small loss of acceptance, the analogue signals of all ten crystals in a row were added and these row sums were discriminated. The 36 row sum signals were used by the logic of the "geometry box" to determine if any two nonadjacent rows had fired within ± 15 ns of each other. In such an event one had a "2γ trigger," the TDC's on each crystal and hodoscope counter were started, and their ADC's were gated. The TDC's were stopped by the delayed individual signals and the detector electronics were read out by the computer.

The $1e$ trigger required coincident pulses in a NaI row sum and its corresponding hodoscope counter, indicating an energetic charged particle. Furthermore, the total energy deposition in the Crystal Box was required to be above about 15 MeV by appropriately discriminating the analogue sum over all NaI channels. This $1e$ trigger caused a full readout of the Crystal Box TDC's and ADC's.

For energy calibration of the NaI crystals a single photon in a given Crystal Box face with an energy deposition of at least 2 MeV was required. This allowed detection of the γ's from the calibration sources as well as of the μ^-Bi x rays. The calibration procedure was carried out separately for each face.

To calibrate the relative timing of all NaI crystals and of all hodoscope counters, the μ^+ beam was directly admitted into the Crystal Box and stopped in a centrally positioned target counter, a 7.6-cm-diam, 0.16-cm-thick scintillator. A charged particle depositing at least 15 MeV in one face in coincidence with a pulse from the target counter at the center of the detector indicated the observation of an energetic e^+ from μ^+ decay in the target counter. Each crystal and hodoscope counter in this quadrant stopped its TDC if a decay e^+ passed through it. The TDC stops for each channel were accepted once promptly and once delayed by a calibrated amount of 10 ns in alternating sequence. These data were used to align the timing offsets and to determine the time bin sizes for all crystals and hodoscope counters. The precise time calibration of the individual scintillators was an important input to the data analysis.

F. Bi targets and secondary electron detector

About half of the $M \rightarrow \overline{M}$ data were taken with a target made by evaporating (1.0 ± 0.2)-μm Bi onto a 50-μm aluminized Mylar foil that was stretched and glued to a 38-cm-diam aluminum ring. This Bi layer was calculated to be thick enough to stop the $M(\overline{M})$ atoms using existing stopping power and range data for hydrogen [44] and the velocity scaling rule. For the other half of the data, a similar target was used which had an additional (7.5 ± 2.5)-nm layer of MgO evaporated on its upstream surface. The thickness of this layer was chosen to allow incident $M(\overline{M})$ atoms to pass through it while enhancing the yield of secondary electrons (SE's) due to their impact. The secondary emission coefficients, γ, of the coated and uncoated Bi target materials were measured in an auxiliary experiment at Oak Ridge National Laboratory [45]. We determined $\gamma = (5.2 \pm 0.2)$ for the coated and $\gamma = (2.8 \pm 0.2)$ for the uncoated targets using protons at 20 keV of kinetic energy, which simulates conditions for beam foil M.

The SE's liberated from the Bi target upon $M(\overline{M})$ impact were accelerated and focused onto the MCP detector located 25 cm upstream of the Bi target. The MCP [46] consisted of a chevron pair of channel plates with 8°/8° channel bias angles. Each plate was 1 mm thick with a 75-mm active area diameter. The channel diameter was 25 μm with a 55% open area ratio. The MCP detector was operated at a voltage of 780 V per plate. A few millimeters in front of the plates, a 95% transparent Cu mesh of the same diameter as the plates, and a 99.5% transparent wire frame ring (with 25-μm gold-plated tungsten wires) of 8 cm inner diameter and 40 cm outer diameter were mounted in order to apply the electric field for collection and acceleration of the SE's (see Fig. 7).

The Bi target and the vacuum pipe were grounded and 300 and 1800 V were applied to the W wire frame guide electrode and to the Cu accelerating mesh, respectively. The POISSON code [47] was used to calculate the electric field in the region between the Bi target and the MCP. A

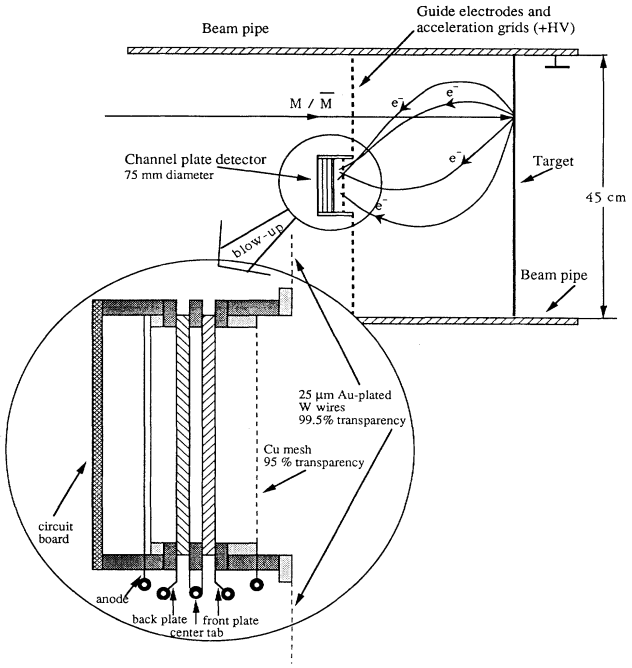

FIG. 7. A detail of the target region showing the secondary emission detector. Some SE trajectories resulting from incoming M or $\overline{M}$ atoms are indicated. A focus on the MCP assembly is given in the closeup.

Monte Carlo simulation of the transport of secondary electrons from the target to the MCP was used to determine the best choice of geometry and of applied voltages, giving a collection efficiency of 90% and a time-of-flight spread of 30–120 ns at optimum [28]. For those runs taken with the 19 MeV/c μ^- beam to study the muonic x-ray detection efficiency, a Bi target of 8 cm×8 cm area and of 150 μm thickness was used to stop the μ^-.

IV. MEASUREMENTS AND DATA ANALYSIS

To search for the $M \rightarrow \overline{M}$ conversion, the full incident μ^+ rate at 10 MeV/c from the SMC was used to form as many M atoms as possible. The incident μ^+ rate and the M production fraction were monitored by the beam counter and by the observation of decay e^+ in the Crystal Box NaI crystals and scintillator hodoscope. A full readout of the Crystal Box detector was triggered whenever at least two photons in nonadjacent rows of NaI crystals were observed. The application of the remaining criteria that would indicate the observation of an $\overline{M}$ atom was reserved for the off-line analysis. These requirements include the presence of a correlated pulse in the SE detector, a minimum opening angle of 30° between the two photons, and the proper energies of the photons.

The coupling constant $G_{M\overline{M}}$ is obtained from the experimentally measured quantities by equating the quotient of the number of $\overline{M}$ atoms, $N_{\overline{M}}$, and the number of M atoms, N_M, at the Bi target, to the time-averaged conversion probability $\langle P(\overline{M}) \rangle_t$ of Eq. (8):

$$\langle P(\overline{M}) \rangle_t = \frac{N_{\overline{M}}}{N_M + N_{\overline{M}}} \simeq \frac{N_{\overline{M}}}{N_M} \ . \tag{9}$$

In the experiment, the number of $\overline{M}$ atoms was obtained from a quotient of the number of triple coincidences and the detector efficiencies according to

$$N_{\overline{M}} = \frac{N_{K\alpha L\alpha \mathrm{SE}}}{\varepsilon_{K\alpha L\alpha/\mu^-} \varepsilon_{\mathrm{SE}}} \ , \tag{10}$$

where $N_{K\alpha L\alpha \mathrm{SE}}$ is the number of coincident μ^-Bi $K\alpha$ and $L\alpha$ photons (detected by the Crystal Box) and SE's (detected by the MCP). The efficiency of the Crystal Box for detecting the μ^- on the Bi target *via* the emission of $K\alpha$ and $L\alpha$ muonic x rays is denoted by $\varepsilon_{K\alpha L\alpha/\mu^-}$, whereas $\varepsilon_{\mathrm{SE}}$ is the efficiency for observing a secondary electron pulse on the MCP upon the impact of an M or $\overline{M}$ atom on the Bi target.

The number of M atoms was obtained similarly from

$$N_M = \frac{N_{e^+\mathrm{SE}}}{\varepsilon_{e^+/M} \varepsilon_{\mathrm{SE}}} \ , \tag{11}$$

where $N_{e^+\mathrm{SE}}$ is the number of positrons from M decay measured by the Crystal Box requiring that the SE pulse caused by M impact on the target was detected by the MCP. The efficiency of detecting a decay e^+ in the Crystal Box per M atom stopping in the target, $\varepsilon_{e^+/M}$, was calculated by a Monte Carlo program to be

$$\varepsilon_{e^+/M} = (51.7 \pm 0.3)\% \ . \tag{12}$$

It should be noted that $\varepsilon_{\mathrm{SE}}$ is taken to be the same for M and $\overline{M}$ atoms and therefore it cancels in taking the ratio of Eq. (9). Nevertheless, it is important to calculate $\varepsilon_{\mathrm{SE}}$ as its magnitude determines the signal-to-background ratio and, hence, the sensitivity of the experiment (see Sec. IV B).

A. Detection efficiency for muonic x rays

With an incident 19-MeV/c μ^- beam, the coincident μ^-Bi $K\alpha$ and $L\alpha$ photons were observed with the Crystal Box triggered by two coincident photons ($\Delta t = 30$ ns) in nonadjacent rows of crystals (2γ trigger). Some of these data were acquired with the additional trigger condition of a correlated μ^- pulse in the beam counter. The nonadjacent row hardware criterion ensured that no false trigger resulted from the energy of a single photon "leaking" into neighboring crystals. A software cut requiring the opening angle of the two photons to be greater than 30° increased the signal-to-background ratio by a factor of 1.7. The background was primarily due to correlated γ rays originating from neutron capture on NaI. The resulting measured spectrum is shown in Fig. 8(a) together with a Monte Carlo generated spectrum in Fig. 8(b). A comparison indicates that the two muonic x rays were observed with little background and that the line shapes were well understood. The measured energies of the $L\alpha$ and $K\alpha$ μ^- Bi x rays are in agreement with the established values [48] ($E_{L\alpha} = 2.61$ MeV and $E_{K\alpha} = 5.97$ MeV) and confirm our energy calibration.

The detection efficiency $\varepsilon_{K\alpha L\alpha/\mu^-}$, including the nonadjacent row and the 30° opening angle requirements, was measured to be

$$\varepsilon_{K\alpha L\alpha/\mu^-}=\frac{N_{K\alpha L\alpha}}{N_{\mu^-}}=(7.5\pm0.6)\% \ , \tag{13}$$

where the number of coincident $K\alpha$ and $L\alpha$ photons, $N_{K\alpha L\alpha}$, was obtained from the spectrum in Fig. 8(a) by a least-squares-fitting procedure. The distribution of the signal was taken from Monte Carlo results [Fig. 8(b)]. The background distribution, shown in Fig. 8(c), was obtained from events taken with the μ^- beam and the requirement that the beam counter did not give a muon pulse correlated to the trigger.

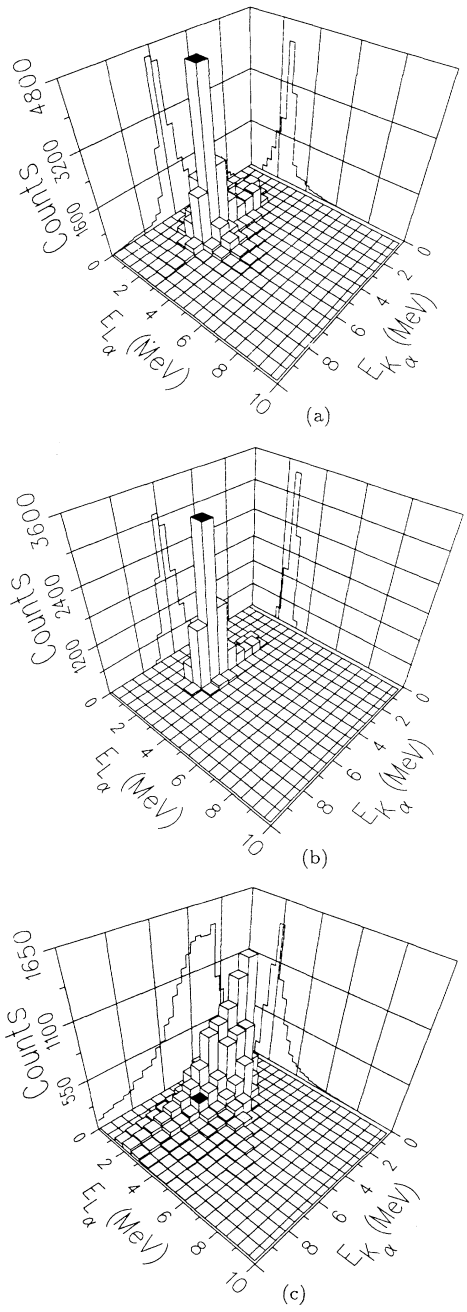

FIG. 8. The 2γ energy spectra from (a) μ^- data, from (b) Monte Carlo data, and (c) the background during the μ^- runs. The shaded bin is centered at $E_{K\alpha}=6.0$ MeV and $E_{L\alpha}=2.6$ MeV with the bin width equal to 0.6 MeV for both dimensions. For the projections on both the $E_{K\alpha}$ and the $E_{L\alpha}$ axes, the bin width is 0.3 MeV.

The number of μ^- stopping in the Bi target, N_{μ^-}, was obtained from the number of μ^- at the beam counter corrected by the measured μ^- transmission efficiency from the beam counter to the Bi target. The transmission efficiency was obtained by replacing the Bi target with the target counter (see Sec. III E) and measuring the number of μ^- detected in the beam counter and the number of μ^- observed in both the beam counter and the target counter. Since the beam profile was not available, a uniform beam distribution at the Bi target was assumed (other plausible assumptions, such as a Gaussian distribution, would increase the transmission efficiency) and a transmission efficiency of $\sim 2.8\%$ was deduced taking into account that the area of the Bi target was 1.49 times that of the target counter.

The efficiency $\varepsilon_{K\alpha L\alpha/\mu^-}$ was also estimated using the Monte Carlo program. Including the nonadjacent row requirement and the 30° opening angle cut, it was found that 10.2% of the $K\alpha, L\alpha$ photon pairs thrown isotropically from the 38-cm-diam Bi target are detected by the Crystal Box. Taking into account the 82% probability [49] that the atomic cascade produces the $K\alpha, L\alpha$ pair, $\varepsilon_{K\alpha L\alpha/\mu^-}=(8.3\pm0.2)\%$ is expected.

The calculated efficiency is higher than the measured one [Eq. (13)] because of crystal-to-crystal variations of trigger thresholds and the possible depletion of the $K\alpha$ yield by a radiationless transition from the $2P$ state to nuclear capture [50] of μ^-, neither of which were considered in the Monte Carlo program. To be conservative, the measured detection efficiency was used in the analysis.

B. Measurement of SE transit time and SE detector efficiency

The proper coincidence window between the two muonic x rays and the SE's was established by measuring the SE transit time from the Bi target to the MCP. This part of the experiment was performed with a 13-MeV/c μ^+ beam and the components of the apparatus set to beam-foil production of muonium. Figure 9 shows the data for the transit time T, the time difference between a MCP signal and a NaI signal, for M incident on the Bi/MgO target. The Crystal Box was triggered on the presence of a single charged particle with energy greater than 15 MeV ($1e$ trigger). The small prompt peak, at $T=0$, is caused by events in which one particle (presumably a positron) hit both the MCP and the Crystal Box. The broad peak, from $T=45$ to 105 ns, is caused by the SE's liberated from the target by energetic decay positrons emerging from it. This is essentially the SE transit time distribution since it took only a few nanoseconds for the positrons to travel from the Bi target to the Crystal Box. This SE transit time was also calculated by a Monte

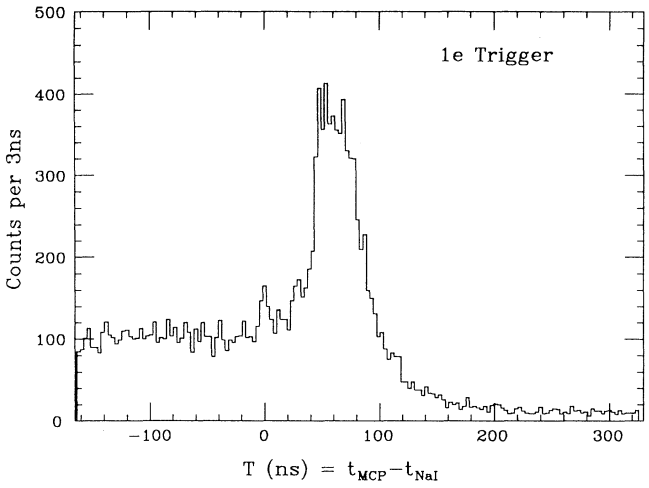

FIG. 9. Time difference between the 1e trigger and the SE's. The TDC was started by the 1e trigger and stopped by the SE detector.

Carlo simulation which gave a result of about 30–120 ns (see Sec. III F). The events with negative T are caused by SE's liberated from the target by the impinging M atoms. Since the M atoms have a lifetime of 2.2 μs, most of their decay positrons were recorded after the detection of the SE's by the MCP.

These data were used to obtain the SE detector efficiency ε_{SE}. For this, two quantities had to be determined: the number of positrons in the Crystal Box with a correlated signal in the MCP, $N_{NaI\,SE}$, and the number without the MCP requirement, N_{NaI}. The number $N_{NaI\,SE}$ was obtained by a least-squares fit to the NaI(Tl) energy spectrum in the time window between $-160 < T < 45$ ns. These are events where a muonium atom on the Bi target preceded a MCP count [see Fig. 10(a)]. This number of counts was then corrected for the portion of the muon lifetime observed. The fit used a flat background and decay e^+ energy distribution parameters obtained from the data taken with a μ^+ beam incident on the target. The number N_{NaI} was obtained by the same fitting routine for the energy spectrum, however, without applying a time window cut [see Fig. 10(b)] and assuming both flat and exponential background terms. The fitted results are shown as smooth lines. The SE detection efficiency for the Bi/MgO target was thus measured to be

$$\varepsilon_{SE} = N_{NaI\,SE}/N_{NaI} = (50.5 \pm 0.7)\% \ . \quad (14)$$

For the uncoated Bi target, the efficiency was a third of this value.

C. Detection of muonium

As given in Eq. (9), the conversion probability of M into $\bar{M}$ is the ratio of the number of $\bar{M}$ counts ($N_{\bar{M}}$) to the number of M counts (N_M) accumulated on the Bi target during the integrated time that data taking was sensitive to the presence of $\bar{M}$. Information proportional to N_M was obtained by a scaler counting the delayed coincidences of 10-μs width between the MCP and a single electron gate of the Crystal Box. This M scaler was calibrated as follows.

The muon beam, the apparatus, and the Crystal Box trigger were maintained in the conditions described in the previous section. Using the 1e trigger, the time difference between a MCP signal and a NaI signal was measured us-

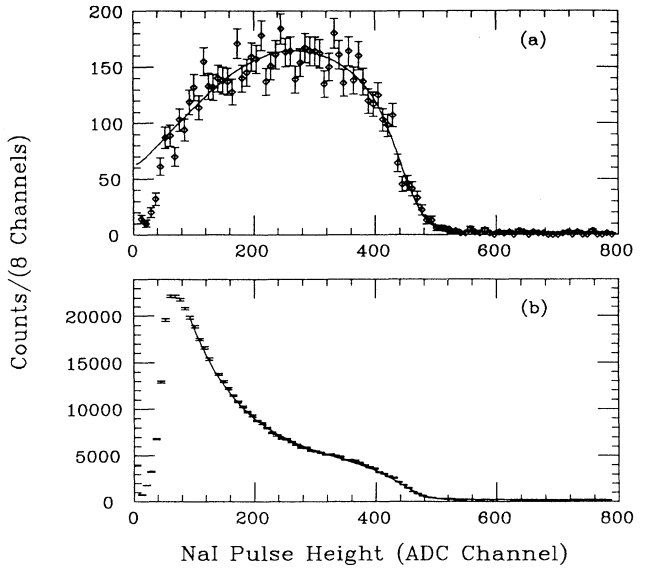

FIG. 10. (a) Data (dots with errors) and fit (smooth curve) of NaI pulse height spectra with $-106 < T < 45$ ns cut where T is the time difference between the 1e trigger and the SE's. (b) Data (dots with errors) and fit (smooth curve) of NaI pulse height without T cut.

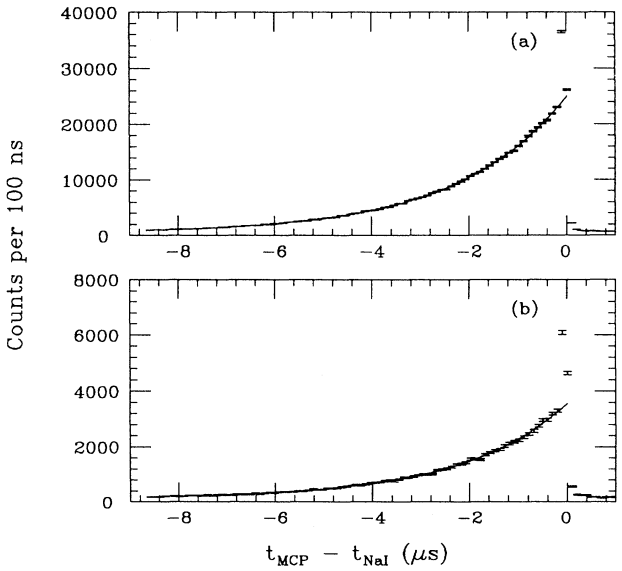

FIG. 11. Part of data (dots with errors) and fit (smooth curve) of TPHC spectra taken (a) with a Bi/MgO target and (b) with a Bi target.

ing a time-to-pulse-height converter (Ortec 467 TPHC), with the full scale range set to 10 μs, connected to a multichannel analyzer (Canberra 35+ MCA). The measured spectra from part of the data are shown in Figs. 11(a) and 11(b) with the Bi/MgO and the Bi targets, respectively. The spectra clearly show the characteristic muon decay, and a least-squares fit indicates a (2.20 ± 0.01)-μs and a (2.16 ± 0.02)-μs muon decay lifetime for the Bi/MgO and the Bi target runs, respectively. The signal-to-background ratio in these histograms is larger and is assumed to be the same as that for the M scaler. Thus, the total counts in this scaler for each target were background subtracted using the fit to the relevant lifetime histogram, giving the total number of M atoms formed during the $\overline{M}$ search. The total number of decay positrons from M decay detected by the Crystal Box with the correlated SE's detected by the MCP, after normalizing to $\overline{M}$ data taking time *via* the M scaler ($\sim$150 h, see next section), was found to be

$$N_{e^+\mathrm{SE}}=(1.18\pm0.07)\times10^6 \ . \tag{15}$$

D. Detection of antimuonium

The $\overline{M}$ atoms were sought during the greater part of the data acquisition time with the Crystal Box in the 2γ trigger mode. The same trigger was already implemented when μ^-Bi x rays were observed with the μ^- beam except that the beam counter signal was removed from the trigger logic for the $\overline{M}$ search. This was done because the $M/\overline{M}$ atoms were moving too slowly (with a correspondingly wide time-of-flight range) for this signal to provide a useful gate.

In the 150 h of data taken to search for the conversion, there were about 6.5×10^6 hardware triggers of which 3.6×10^6 events remained after the 30° opening angle cut in software. The overwhelming majority of these events were not accompanied by a delayed coincidence of SE's from the Bi target with a 300-ns range. The distribution of the time difference $T=(t_{\mathrm{MCP}}-t_{\mathrm{NaI}})$ for events with a MCP coincidence is shown in Fig. 12. The calibration of the time interval from the arrival of an M atom to the response of the SE detector indicates that the good $\overline{M}$ events are expected to fall into the $35<T<115$ ns range, which was chosen 10 ns wider on each side compared to Fig. 9. Only 1787 events survived this requirement. The background-dominated sample was thus reduced by a factor of 2×10^3 at the expense of a 50% decrease in acceptance for M and for $\overline{M}$. The energy distribution of the 1787 events is shown in Fig. 13. No structure near $E_{K\alpha}=6.0$ MeV and $E_{L\alpha}=2.6$ MeV is visible, which indicates that no statistically significant μ^- Bi x rays were observed.

The quantity $N_{K\alpha L\alpha\mathrm{SE}}$ was determined by a maximum-likelihood analysis. We assumed that, among the 1787 remaining events, there are some number of $\overline{M}$ events and two types of background events.

Type-1 background is due to M (i.e., μ^+) decays in the Bi target. A decay e^+ liberates SE's from the target when leaving it. Because of the incomplete rejection of charged particles by the hodoscope veto, the e^+ pulse in a NaI channel may give a 2γ trigger *via* an accidental coincidence with single photon counts from neutron capture or it may generate bremsstrahlung photons when passing through the materials inside the Crystal Box. Thus, type-1 background leads to counts in the broad TOF peak in Fig. 12.

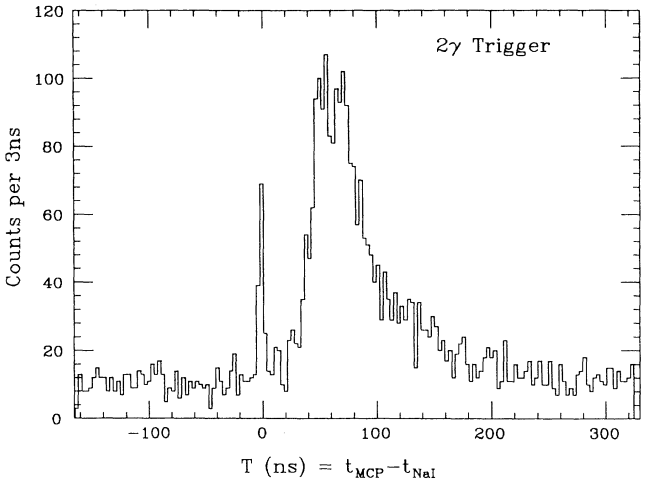

FIG. 12. Time difference between the 2γ trigger and the SE's. The TDC was started by the 2γ trigger and stopped by the SE detector.

Type-2 background events have no correlated SE's and are flatly distributed in Fig. 12. The origin of these events is the generation of correlated γ rays from neutron capture in the NaI crystals in accidental coincidence with a background count in the SE detector, which we attribute to thermionic emission of electrons from the target surface. Another possible contribution is the decay of μ^+ from M stopping elsewhere than in the Bi target and causing a 2γ trigger as described above for type-1 background, however, in accidental coincidence with a SE detector count.

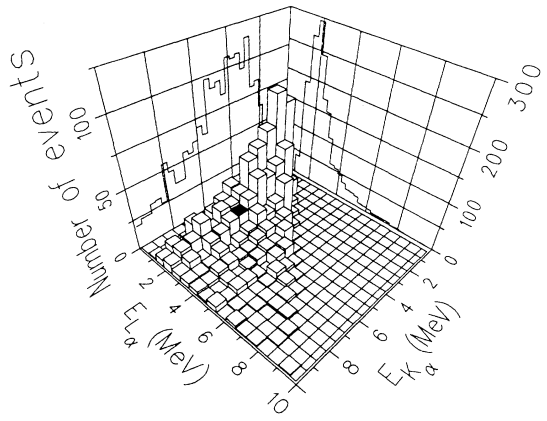

FIG. 13. Energy spectrum of the two photons for the sum of all data taken in search of $\overline{M}$. The cuts applied are (1) an opening angle between the photons of greater than 30° and (2) $35<T<115$ ns, where T is the time difference between a two-photon signal and a SE signal. The binning is chosen as in Fig. 8.

The normalized two-dimensional probability distributions for these three sources of events were used to construct the likelihood function. The parameters of these distributions are the measured photon energies for an event, where the higher energy is labeled as $E_{K\alpha}$ and the lower energy as $E_{L\alpha}$.

The $\overline{M}$ probability distribution, $S(\mathbf{X})$, with $\mathbf{X}=(E_{K\alpha},E_{L\alpha})$, shown in Fig. 8(b), was generated by the Monte Carlo program. Because the type-1 background events were M related, its probability distribution, $B_1(\mathbf{X})$, was determined by the effects of the decay positrons from M atoms. This background was efficiently simulated by stopping a μ^+ beam directly in the Bi target and acquiring data with the 2γ trigger. The distribution $B_1(\mathbf{X})$ was then obtained by requiring a minimum opening angle of 30° between the two γ's and the presence of a SE detector count, as was applied to extract the 1787 candidate events. The type-2 background distribution $B_2(\mathbf{X})$ was generated from 2% of the 3.6×10^6 events that survived the 30° angle cut.

The likelihood function is written as

$$L(N_{K\alpha L\alpha SE},N_1,N_2)$$

$$=\prod_{i=1}^{N}\frac{1}{N}[N_{K\alpha L\alpha SE}S(\mathbf{X})+N_1B_1(\mathbf{X})+N_2B_2(\mathbf{X})] \quad (16)$$

with the condition

$$N=N_{K\alpha L\alpha SE}+N_1+N_2=1787\ . \quad (17)$$

The likelihood $L(N_{K\alpha L\alpha SE},N_1,N_2)$ was calculated as $N_{K\alpha L\alpha SE}$ and N_1 were varied. The maximum of $L(N_{K\alpha L\alpha SE},N_1,N_2)$ was found at $N_{K\alpha L\alpha SE}=-3$ and $N_1=1400$, indicating that the distribution is consistent with the absence of any $\overline{M}$ events among the 1787 candidate events. The projection of $L(N_{K\alpha L\alpha SE},N_1,N_2)$ onto $N_{K\alpha L\alpha SE}$, shown in Fig. 14 implies

$$N_{K\alpha L\alpha SE}<20 \quad (90\%\ \text{C.L.})\ . \quad (18)$$

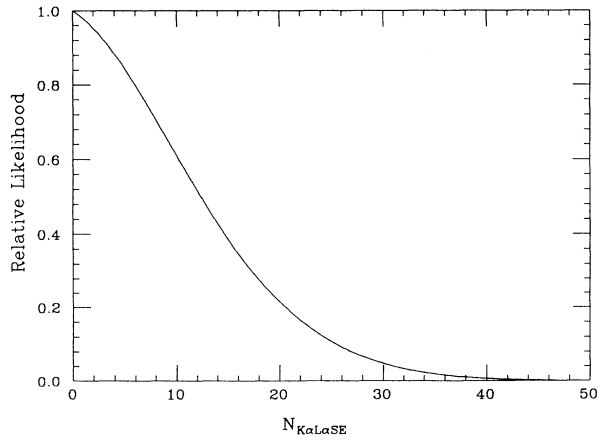

FIG. 14. Normalized likelihood function vs the number of $\overline{M}$ events.

Because there could be a small contamination of $\overline{M}$-induced events in the type-2 background distribution, a signal corresponding to $G_{M\overline{M}}=20G_F$ (the previous best upper limit [21]) was subtracted from $B_2(\mathbf{X})$ and $L(N_{K\alpha L\alpha SE},N_1,N_2)$ was maximized again. The final result was found to be unaffected by replacing the original $B_2(\mathbf{X})$ with the signal-subtracted $B_2(\mathbf{X})$.

The maximum-likelihood analysis was checked by calculating the likelihood function on a data sample in which ten events, generated according to the $\overline{M}$ signal distribution, were added into the 1787 events. The $L(N_{K\alpha L\alpha SE},N_1,N_2)$ then peaked at $N_{K\alpha L\alpha SE}=10$ which shows that the program would have found any $\overline{M}$ events, had they existed in the data sample.

V. RESULTS AND DISCUSSION

A comparison of Eqs. (8) and (9) for $\langle P(\overline{M})\rangle_t$, using the quantities in Eqs. (10)–(18), results in the upper limit

$$\langle P(\overline{M})\rangle_t<1.2\times10^{-4}\ , \quad (19)$$

which leads to a limit of

$$G_{M\overline{M}}<6.9G_F \quad (90\%\ \text{C.L.}) \quad (20)$$

on the coupling constant in an effective V-A contact interaction. This value represents a factor of 3 improvement over the previous result [21]. This was the first experiment sensitive enough to probe couplings for which a left-right-symmetric theory with a doubly charged Higgs triplet may produce the $M\rightarrow\overline{M}$ conversion.

The triple coincidence signature used is powerful in suppressing background from correlated γ's from neutron capture on NaI. However, the experiment is limited by processes that cause SE counts correlated to at least one other photon and in accidental coincidence with a single neutron capture γ, which is the main contribution to the singles rate of low-energy γ's in the NaI crystals. Further constraints on the sensitivity are imposed by the relatively short time (~1 μs) during which a conversion was possible (the TOF from the production foil to the target) and by the small solid angle subtended by the Bi target at the M production foil. The neutrons are produced by the proton beam of the LAMPF linac as it interacts with the pion production targets in the experimental area. As the shielding of the detector against neutrons was already elaborate, little improvement could be expected from attempts to further extend it. The small solid angle of the target foil with respect to the M production foil is a direct consequence of the need for a

non-negligible flight time of the M atoms during which a conversion to $\bar{M}$ might occur. The flight path chosen and the resulting solid angle of the target foil represents a compromise between these two competing criteria.

ACKNOWLEDGMENTS

We acknowledge the assistance of the members of the Crystal Box group and of the Los Alamos Meson Physics Facility staff. Special thanks go to C. J. Barnett,[1] B. Barthell, J. Germani, J. Ivie, D. C. Lu, J. McDonough, N. Meyer, and L. Trudell. This work was supported in part by the U.S. Department of Energy, the U.S. National Science Foundation, and the Bundesministerium für Forschung und Technologie of the Federal Republic of Germany.

[1]Deceased.

[1] B. Pontecorvo, Zh. Eksp. Teor. Fiz. **33**, 549 (1957) [Sov. Phys. JETP **6**, 429 (1958)].
[2] G. Feinberg and S. Weinberg, Phys. Rev. Lett. **6**, 381 (1961).
[3] J. Schwinger, Ann. Phys. (N.Y.) **2**, 407 (1957).
[4] K. Nishijima, Phys. Rev. **108**, 907 (1957).
[5] S. A. Bludman, Nuovo Cimento **9**, 433 (1958).
[6] S. L. Glashow, Nucl. Phys. **22**, 579 (1961).
[7] A. Salam, in *Elementary Particle Theory: Relativistic Groups and Analyticity (Nobel Symposium No. 8),* edited by N. Svartholm (Almqvist and Wiksell, Stockholm, 1968), p. 367.
[8] S. Weinberg, Phys. Rev. Lett. **19**, 1264 (1967); **27**, 1688 (1968).
[9] J. C. Pati and A. Salam, Phys. Rev. D **10**, 275 (1974).
[10] H. Fritzsch and P. Minkowski, Nucl. Phys. **B103**, 61 (1976).
[11] R. N. Mohapatra and D. P. Sidhu, Phys. Rev. Lett. **38**, 667 (1977).
[12] R. N. Mohapatra and G. Senjanovic, Phys. Rev. D **23**, 165 (1981); P. Herczeg and R. N. Mohapatra, in *The Vancouver Meeting—Particles and Fields '91,* Proceedings of the Joint Meeting of the Division of Particles and Fields of the American Physical Society and the Particle Physics Division of the Canadian Association of Physicists, Vancouver, 1991, edited by D. Axen, D. Bryman, and M. Comyn (World Scientific, Singapore, 1992), Vol. 1, p. 572; G. B. Gelmini and M. Roncadelli, Phys. Lett. **99B**, 411 (1981); D. Chang and W.-Y. Keung, Phys. Rev. Lett. **62**, 2583 (1989); M. L. Swartz, Phys. Rev. D **40**, 1521 (1989).
[13] S. P. Rosen, in *Neutrino '81,* Proceedings of the International Conference on Neutrino Physics and Astrophysics, Weilea, Hawaii, 1981, edited by R. J. Cence, E. Ma, and A. Roberts (University of Hawaii, Honolulu, 1981), p. 76.
[14] A. Halprin, Phys. Rev. Lett. **49**, 1313 (1982).
[15] B. Ni, K.-P. Arnold, F. Chmely, V. W. Hughes, S. H. Kettell, Y. Kuang, J. Markey, B. E. Matthias, H. Orth, H. R. Schaefer, K. Woodle, M. D. Cooper, C. M. Hoffman, C. E. Hogan, R. E. Mischke, L. E. Piilonen, R. A. Williams, M. Eckhause, P. Guss, J. Kane, J. Reidy, and G. zu Putlitz, Phys. Rev. Lett. **59**, 2716 (1987); in *PANIC '87,* Proceedings of the Eleventh International Conference on Particles and Nuclei, Kyoto, Japan, 1987, edited by S. Homma *et al.* [Nucl. Phys. **A478**, 757c (1988)].
[16] P. R. Bolton, A. Badertscher, P. O. Egan, C. J. Gardner, M. Gladisch, V. W. Hughes, D. C. Lu, M. Ritter, P. A. Souder, J. Vetter, G. zu Putlitz, M. Eckhause, and J. Kane, Phys. Rev. Lett. **47**, 1441 (1981).
[17] J. J. Amato, P. Crane, V. W. Hughes, J. E. Rothberg, and P. A. Thompson, Phys. Rev. Lett. **21**, 1709 (1968).
[18] D. L. Morgan, Ph.D. thesis, Yale University, 1966.
[19] W. C. Barber, B. Gittelman, D. C. Cheng, and G. K. O'Neill, Phys. Rev. Lett. **22**, 902 (1969).
[20] G. M. Marshall, J. B. Warren, C. J. Oram, and R. F. Kiefl, Phys. Rev. D **25**, 1174 (1982).
[21] G. A. Beer, G. M. Marshall, G. R. Mason, A. Olin, Z. Gelbart, K. R. Kendall, T. Bowen, P. G. Halverson, A. E. Pifer, C. A. Fry, J. B. Warren, and A. R. Kunselman, Phys. Rev. Lett. **57**, 671 (1986).
[22] K. A. Woodle, K.-P. Arnold, M. Gladisch, J. Hofmann, M. Janousch, K. P. Jungmann, H.-J. Mundinger, G. zu Putlitz, J. Rosenkranz, W. Schäfer, G. Schiff, W. Schwarz, V. W. Hughes, and S. H. Kettell, Z. Phys. D **9**, 59 (1988).
[23] A. C. Janissen, G. A. Beer, G. R. Mason, A. Olin, T. M. Huber, A. R. Kunselman, T. Bowen, P. G. Halverson, C. A. Fry, K. R. Kendall, G. M. Marshall, and J. B. Warren, Phys. Rev. A **42**, 161 (1990).
[24] T. M. Huber, A. R. Kunselman, A. C. Janissen, G. A. Beer, G. R. Mason, A. Olin, T. Bowen, P. G. Halverson, C. A. Fry, K. R. Kendall, G. M. Marshall, B. Heinrich, K. Myrtle, and J. B. Warren, Phys. Rev. D **41**, 2709 (1990).
[25] B. E. Matthias, H. E. Ahn, A. Badertscher, F. Chmely, M. Eckhause, V. W. Hughes, K. P. Jungmann, J. R. Kane, S. H. Kettell, Y. Kuang, H.-J. Mundinger, B. Ni, H. Orth, G. zu Putlitz, H. R. Schaefer, M. T. Witkowski, and K. A. Woodle, Phys. Rev. Lett. **66**, 2716 (1991).
[26] G. Feinberg and S. Weinberg, Phys. Rev. **123**, 1439 (1961).
[27] B. E. Matthias, Ph.D. thesis, Yale University, 1991.
[28] B. Ni, Ph.D. thesis, Yale University, 1989.
[29] P. A. Thompson, V. W. Hughes, W. P. Lysenko, and H. F. Vogel, Nucl. Instrum. Methods **161**, 391 (1979).
[30] H. E. Ahn, Ph.D. thesis, Yale University, 1992.
[31] R. D. Bolton, M. D. Cooper, J. S. Frank, A. L. Hallin, P. A. Heusi, C. M. Hoffman, G. E. Hogan, F. G. Mariam, H. S. Matis, R. E. Mischke, L. E. Piilonen, V. D. Sandberg, G. H. Sanders, U. Sennhauser, R. Werbeck, R. A. Williams, S. L. Wilson, R. Hofstadter, E. B. Hughes, M. W. Ritter, D. Grosnick, S. C. Wright, V. L. Highland, and J. McDonough, Phys. Rev. D **38**, 2077 (1988).
[32] A. Badertscher, P. O. Egan, M. Gladisch, M. Greene, V. W. Hughes, F. G. Mariam, D. C. Lu, G. zu Putlitz, M. W. Ritter, G. Sanders, P. A. Souder, and R. Werbeck, Nucl. Instrum. Methods **238**, 200 (1985).
[33] J. B. Donahue, LAMPF Internal Report, 1983 (unpublished).
[34] C. J. Oram, J. M. Bailey, P. W. Schmor, C. A. Fry, R. F. Kiefl, J. B. Warren, G. M. Marshall, and A. Olin, Phys. Rev. Lett. **52**, 910 (1984).
[35] A. Badertscher, S. Dhawan, P. O. Egan, V. W. Hughes, D. C. Lu, M. W. Ritter, K. A. Woodle, M. Gladisch, H.

Orth, G. zu Putlitz, M. Eckhause, J. Kane, F. G. Mariam, and J. R. Reidy, Phys. Rev. Lett. **52**, 914 (1984).

[36] Y. Kuang, K.-P. Arnold, F. Chmely, M. Eckhause, V. W. Hughes, J. R. Kane, S. Kettell, D.-H. Kim, K. Kumar, D. C. Lu, B. Matthias, B. Ni, H. Orth, G. zu Putlitz, H. R. Schaefer, P. A. Souder, and K. Woodle, Phys. Rev. A **39**, 6109 (1989).

[37] K. A. Woodle, A. Badertscher, V. W. Hughes, D. C. Lu, M. W. Ritter, M. Gladisch, H. Orth, G. zu Putlitz, M. Eckhause, J. Kane, and F. G. Mariam, Phys. Rev. A **41**, 93 (1990).

[38] S. H. Kettell, Ph.D. thesis, Yale University, 1990.

[39] A. Badertscher, V. W. Hughes, D. C. Lu, M. W. Ritter, K. A. Woodle, M. Gladisch, H. Orth, G. zu Putlitz, M. Eckhause, J. Kane, and F. G. Mariam, in *Atomic Physics 9,* Proceedings of the Ninth International Conference, Seattle, Washington, 1984, edited by Robert S. Van Dyck, Jr. and E. Norval Fortson (World Scientific, Singapore, 1984), p. 83.

[40] J. A. Phillips, Phys. Rev. **97**, 404 (1955).

[41] K. H. Berkner, I. Bornstein, R. V. Pyle, and J. W. Stearns, Phys. Rev. A **6**, 278 (1972).

[42] R. S. Bhattacharya, W. Eckstein, and H. Verbeek, Surf. Sci. **93**, 563 (1980).

[43] W. Eckstein and F. E. P. Matschke, Phys. Rev. B **14**, 3231 (1976).

[44] H. H. Anderson and J. F. Ziegler, *Hydrogen Stopping Powers and Ranges in All Elements* (Pergamon, New York, 1977).

[45] C. F. Barnett, F. Chmely, V. W. Hughes, S. H. Kettell, Y. Kuang, B. E. Matthias, B. Ni, and H. Orth, Bull. Am. Phys. Soc. **32**, 1031 (1987).

[46] Galileo Electro-Optics Corporation, Model 3075 CEMA.

[47] M. T. Menzel and H. K. Stokes, "POISSON Group of Code," LANL Report No. LA-UR-87-115 (unpublished).

[48] R. Engfer, H. Schneuwly, J. L. Vuilleumier, H. K. Walter, and A. Zehnder, Atomic Data Nucl. Data Tables **14**, 509 (1974). These tables give the results of several experiments for the energies of each fine-structure component of the muonic x rays. We combined the two fine structure contributions to $K\alpha$ and to $L\alpha$ in Bi with their statistical weights to obtain the peak energies expected in our experiment, where the energy resolution is modest and cannot resolve the fine structure of muonic x rays. These weighted averages are the values given in the text.

[49] F. J. Hartmann, R. Bergmann, H. Daniel, H.-J. Pfeiffer, T. von Egidy, and W. Wilhelm, Z. Phys. A **305**, 189 (1982). A small extrapolation is needed as the measurements in this reference were in Au.

[50] R. J. Powers, Phys. Rev. **169**, 1 (1968).